Colloid and Polymer Science (2018) 296:341–353
https://doi.org/10.1007/s00396-017-4256-9

ORIGINAL CONTRIBUTION

Adsorption of benzyldimethyldodecylammonium bromide on silica nanoparticles in water

Shasha Jiang[1] · Huifang Xu[1] · Na Du[1] · Shue Song[1] · Wanguo Hou[1]

Received: 24 October 2017 / Accepted: 20 December 2017 / Published online: 4 January 2018

Abstract

Adsorption of the cationic surfactant benzyldimethyldodecylammonium bromide (BDDABr) on silica nanoparticles with ~ 12 and 31 nm in size (denoted as S-SiO_2 and L-SiO_2, respectively) is investigated at various solid dosages (C_s, 10–40 g/L), pH (3–10), and temperature (T, 298–308 K). No C_s-effect is observed in the adsorption. However, it is interestingly found that, besides pH and T, the size of the silica particles has an obvious influence on the adsorption. The adsorption may show the Langmuir type (L-type), S-type, and "double plateau" type (LS-type) isotherms, depending on silica particle sizes and pH. Increasing pH may lead to a change in the isotherm types from S-type through LS-type to L-type. The S-type and LS-type isotherms can be adequately described using the one-step and two-step surface micellization models, respectively. The affinity of the S-SiO_2 toward BDDABr is lower than that of the L-SiO_2, consistent with the dissociation tendency of their surface hydroxyl groups.

Keywords Adsorption · Silica · Surfactant · Surface micellization · Particle size

Introduction

Adsorption of surfactants at solid–liquid interfaces has been extensively investigated owing to its fundamental and practical importance [1–7]. For instance, it plays an important role in many technological and industrial applications, such as detergency, mineral flotation, dispersion of solids, and oil recovery [3]. Surface modification of solid adsorbents through surfactant adsorption can significantly enhance their removal efficiency of contaminants from aqueous solutions, showing a good potential for application in wastewater treatment [8–10]. It is well known that the behavior of surfactant adsorption is generally governed by a number of forces, including electrostatic interaction, covalent bonding, hydrogen bonding, hydrophobic effects, and solvation/desolvation [3, 5]. A total adsorption is usually the cumulative result of some or all of these forces, depending on the natures of both surfactants and solid surfaces as well as on the environmental conditions. Therefore, surfactant adsorption is a complex interfacial phenomenon. Three types of adsorption isotherms have been identified, namely, Langmuir type (L-type), S-type, and "double plateau" type (LS-type) isotherms [1]. The L-type isotherm can be described using the classical Langmuir model, while the mechanisms of S-type and LS-type adsorption are complex [1, 5]. To explore the adsorption mechanism and describe the adsorption isotherms, several surface micellization models, such as "one-step" [11], "two-step" [12–14], and "four-region" [15–17], were developed [1–3, 5]. The one-step and two-step models can describe the S-type and LS-type isotherms, respectively, and, more importantly, can provide information of surfactant micellization at solid–liquid interfaces [1, 5, 11–14].

A wide variety of solid adsorbents, such as metal/nonmetal oxides (alumina [9, 15, 18–21], titania [16, 17, 22], iron oxide [23, 24], and silica [4, 25–28]), mineral clays (kaolinite [15, 29] and montmorillonite [29, 30]), polymer beads or films [31–33], carbon materials (activated carbon [34], carbon

Electronic supplementary material The online version of this article (https://doi.org/10.1007/s00396-017-4256-9) contains supplementary material, which is available to authorized users.

✉ Wanguo Hou
wghou@sdu.edu.cn

[1] Key Laboratory of Colloid & Interface Chemistry (Ministry of Education), Shandong University, Jinan 250100, China

nanotubes [35, 36], and graphene nanosheets [36]), and nanocellulose [7], have been used to study the adsorption behavior of surfactants at solid–liquid interfaces. Amorphous silica (SiO_2) is one of the most widely used adsorbents [4, 25–28], which has a lowest point of zero charge (PZC, pH ~2) and unusual surface properties compared to other well-characterized oxide surfaces [2, 3]. There has been a well understanding for the effects of the particle surface features, such as the pore structure and the chemical state of surface hydroxyl groups (or silanol groups, Si-OH), and the environmental conditions, such as pH, temperature, and ionic strength, on the adsorption [11, 27, 28, 37–43]. However, understanding on the effect of particle sizes is still limited, owing to the fact that little attention has been focused on this aspect. To our knowledge, only Penfold's group [44, 45] has investigated the effect of silica sol sizes (~7.8 and 13.8 nm) on the adsorbed layer thickness of the nonionic surfactant alkyl polyoxyethylene ether (C_nEO_m) by using the small-angle neutron scattering (SANS) technique. A difference in the adsorbed layer thickness between the two silica sols was observed, but no information on the adsorption amount and, especially, the adsorption thermodynamics were provided in the studies [44, 45]. In principle, the size (or surface curvature) of adsorbent particles can affect the physicochemical state of their surface molecules or groups, which may affect their adsorption for surfactants from solutions. In addition, there have been some reports focused on the effect of particle sizes on adsorption of polymers and biomolecules at solid–liquid interfaces [46–49]. Greenwood et al. [46] found that the adsorbed layer thickness of the ABA block copolymer Synperonic F127 (PEO-PPO-PEO) on poly(methyl methacrylate) (PMMA) and polystyrene (PS) latexes increased with an increase in the latex particle sizes. Vertegel et al. [47] reported that the adsorbed amount of chicken egg lysozyme on silica nanoparticles increased with the increase of particle size, demonstrating that stronger protein–particle interactions exist in the case of larger nanoparticles. Lindman et al. [48] determined the surface coverage degree of human serum albumin (HSA) on *N*-iso-propylacrylamide/*N*-tert-butylacrylamide (NIPAM/BAM) copolymer nanoparticles with a size range of 70–700 nm; they found that the surface coverage degree on the smaller particles (70 nm) was lower than that on the larger particles (120–700 nm), suggesting that a higher degree of surface curvature interferes with binding of HSA. Recently, Walkey et al. [49] found that the adsorbed surface density of serum protein on gold nanoparticle decreased with an increase in particle sizes. These previous studies clearly demonstrate that adsorbent particle sizes may obviously impact adsorption and the size-effect is complex. Up to now, the size-effect mechanism has been less understood. Therefore, research on particle size dependence of surfactant adsorption at solid–liquid interfaces are very essential, which can deepen our understanding of the adsorption phenomena.

Benzyldimethyldodecylammonium halide ($BDDA^+X^-$, commonly $X^- = Cl^-$ and Br^-) is one kind of quaternary ammonium surfactants and widely applied in clinical, cosmetic, and industrial areas [31, 50–52]. However, research on the aggregation features of $BDDA^+X^-$ in solutions [51, 53, 54] and those at solid–liquid interfaces [31, 37, 39] are scarce. Harkot and Jańczuk [31] studied the effect of BDDABr adsorption on wetting of polytetrafluoroethylene and poly(methyl methacrylate) surfaces. Partyka's group [37, 39] investigated the adsorption of BDDABr on silica particles with a mean size of 130 nm in water at free pH. It is interesting to understand the influence of silica particle sizes on the BDDABr adsorption from aqueous solutions at various pH values.

In the current work, the adsorption of BDDABr on amorphous silica particles with different sizes (~12 and 31 nm, denoted as S-SiO_2 and L-SiO_2, respectively) in water was investigated at various solid dosages (C_s, 10–40 g/L), pH (3–10), and temperature (T, 298–308 K). The original aim of this study is to examine whether the "sorbent concentration effect" (C_s-effect) exists in the adsorption process. The so-called C_s-effect (or "solid effect") is a phenomenon that the adsorption isotherms (or saturation adsorption capacity) decline with increasing C_s under given conditions (such as temperature, pressure, and medium composition) [55, 56]. No C_s-effect was observed in the adsorption systems. However, interestingly, it is found that, besides pH and T, the size of the silica particles has an obvious influence on the adsorption. The affinity of the S-SiO_2 toward BDDABr is lower than that of the L-SiO_2. In addition, we find that the adsorption may show the S-type, LS-type, and L-type isotherms, depending on silica particle sizes and pH. The obtained S-type and LS-type isotherms are analyzed using the one-step and two-step models, and the effect of silica particle sizes on the surface micellization of BDDABr is observed. To the best of our knowledge, this is the first report on the effect of adsorbent particle sizes on adsorption thermodynamic features. We think that this work provides a better understanding of cationic surfactant adsorption at silica–liquid interfaces.

Experimental section

Materials

Two high-purity (≥ 99.5%) silica nanoparticle samples, with average diameters of ~12 and 31 nm, respectively, were purchased from Macklin, China. Benzyldimethyldodecylammonium bromide (BDDABr, ≥ 97% for purity) was purchased from TCI, China, and used as received. Its molecular structure is shown in Fig. S1 in the Electronic Supplementary Material (ESM). All other chemicals used in this work were of analytical reagent grade. Ultrapure water with a resistivity of 18.25 MΩ cm was obtained using a Hitech-Kflow water purification system (Hitech, China).

Acid-base titration

Acid-base titration was performed at 25 °C to determine the surface density (N_s) and apparent dissociation constant (K_a) of surface hydroxyl groups (or silanol groups) of the SiO_2 adsorbents.

Silica particles (0.75 g) were dispersed in 75 mL water under magnetic stirring, and the pH of the suspension was adjusted to be ~2.8 using 1.00 M HCl. Prior to acid-base titration, the resultant suspension was magnetically stirred for 24 h at 25 ± 0.5 °C in an atmosphere of N_2, and its pH was adjusted again if necessary. Afterwards, the suspension was back-titrated using 0.20 mM NaOH in 0.1 mL increments to pH ~ 11.0. During the titration period, N_2 was bubbled to exclude CO_2, the mixture was magnetically stirred, and the temperature was kept at 25 ± 0.5 °C using a HK-2A thermostatic bath (Nanjing Nanda Wanhe Science & Technology Co., Ltd., China). After each addition of the NaOH, the pH value of the suspension and the cumulative volume of the NaOH added were recorded when the change in pH value did not exceed 0.02 pH unit in 5 min. The pH values of the suspension were measured using a FE28 pH meter (Mettler-Toledo Instruments (Shanghai) Co., Ltd., China), calibrated by three buffer solutions with pH 4.00, 6.86, and 9.18. The titration was also performed on the blank system (water) as control. The tests were performed in triplicate, and the final values are the average of the three measurements.

The titration data were analyzed using Gran functions [57, 58] to estimate the N_s value. Two Gran functions, G_a and G_b, were used:

$$G_a = (V_0 + V)\ 10^{-pH} \quad (for\ the\ acidic\ side) \tag{1}$$

$$G_b = (V_0 + V)\ 10^{pH-14} \quad (for\ the\ alkaline\ side) \tag{2}$$

where V_0 (mL) is the start volume of suspension, and V (mL) is the cumulative volume of added NaOH solution. Plots of the Gran functions G_a and G_b versus V can form two straight lines, which intersect the V-axis at V_{eq1} and V_{eq2}, respectively. The difference ($V_{eq2} - V_{eq1}$) is the volume of added NaOH needed to achieve a complete neutralization reaction for the hydroxyl groups of silica surfaces. Notably, the hydroxyl groups of silica surfaces (Sur-OH, here "Sur" represents the surface) cannot be protonated to form protonated hydroxyl groups (Sur-OH_2^+), owing to the PZC of SiO_2 being about pH 2 [3, 38, 39]. Therefore, the N_s (sites/nm^2) of the SiO_2 adsorbents can be estimated by:

$$N_s = \frac{\left[\left(V_{eq2}-V_{eq1}\right)_{sample} - \left(V_{eq2}-V_{eq1}\right)_{control}\right] C_{NaOH} N_A}{mA_s} \times 10^{-24} \tag{3}$$

where C_{NaOH} (mM) is the concentration of NaOH solution, N_A is the Avogadro's number (6.02×10^{23}), m (g) is the used amount of adsorbent, A_s (m^2/g) is the specific surface area of adsorbent, and 10^{-24} is a conversion factor for units.

The pK_a of the SiO_2 was estimated from the titration data via the estimation of the dissociation degree (α_{SH}) of surface hydroxyl groups at various pH. The dissociation reaction of surface hydroxyl groups for SiO_2 can be expressed as:

$$Sur{-}OH \rightleftharpoons Sur{-}O^- + H^+ \tag{4}$$

The apparent equilibrium constant (K_a) of the dissociation reaction is given by:

$$K_a = \frac{[\boldsymbol{Sur{-}O^-}][\boldsymbol{H^+}]}{[\boldsymbol{Sur{-}OH}]} \tag{5}$$

where [Sur-OH] and [Sur-O$^-$] are the surface densities of Sur-OH and Sur-O$^-$ groups, respectively. The α_{SH} of surface hydroxyl groups is defined as:

$$\alpha_{SH} = \frac{[\boldsymbol{Sur{-}O^-}]}{N_s} \tag{6}$$

The [Sur-O$^-$] value at a given pH was calculated by the following:

$$[\boldsymbol{Sur{-}O^-}] = \frac{\left([\boldsymbol{OH^-}]_{control} - [\boldsymbol{OH^-}]_{sample}\right)(V_0 + V)}{A_s m} \tag{7}$$

where $[OH^-]_{control}$ and $[OH^-]_{sample}$ are the OH^- concentrations of the control and test sample systems, respectively, at the V of added NaOH solution. The pK_a value of surface hydroxyl groups for the test samples was given by the pH value at which $\alpha_{SH} = 0.5$ (i.e., [Sur-OH] = [Sur-O$^-$]).

Conductivity measurement

Conductivity (κ) measurements were performed on a DSJ-308A digital conductivity meter (Shanghai REX Instrument Factory, China) with a DJS-1C glass electrode. The temperature of the measurement cell was controlled at 25.0 ± 0.1 °C using the HK-2A thermostatic bath. The tests were performed in triplicate, and the final values are the average of the three measurements.

Characterization of adsorbent

The morphology and size of solid samples were analyzed using a JEM-2100 transmission electron microscopy (TEM, JEOL, Japan) and a JSM-6700F scanning electron microscopy (SEM, JEOL, Japan). The elemental composition of the samples was determined using energy dispersive spectrometer (EDS) equipped in the SEM instrument. Specific surface area (A_s) of the samples was determined by measuring volumetric

N_2 adsorption–desorption isotherms at liquid nitrogen temperature using an Autosorb IQ-MP instrument (Quantachrome Instruments, USA). Samples were degassed at 200 °C for 3 h under vacuum before measurement.

Adsorption experiment

The adsorption experiments were performed using a batch technique at different adsorbent dosages (C_s, 10–40 g/L), BDDABr concentrations (C_i, 0–30 mmol/L), pH (3–10), and temperatures (T, 298, 303, and 308 K). Known masses (0.25–1.00 g) of the adsorbents were added to 25 mL of test BDDABr solutions in polyethylene centrifuge tubes. The centrifuge tubes were shaken using a thermostatic water bath shaker (Jiangsu Medical Instrument Factory, China) for 24 h at a given T. The adsorption kinetic tests showed that the contact time of 24 h was sufficient to reach adsorption equilibrium. The adsorbent particles were then separated from the adsorption systems by centrifugation (GT16-3, Beijing Shidai Beili Centrifuge Co., Ltd., China) at 12,000 rpm for 30 min. The concentrations of BDDABr remaining in the resultant supernatants were determined using UV–vis spectrometry (SP-4100, Shanghai Spectrum Instruments Co., Ltd., China) at 262 nm. The equilibrium adsorption amounts were calculated from the difference between the initial and remaining (or equilibrium) concentrations, using the following equation:

$$\Gamma_e = \frac{C_i - C_e}{C_s} \tag{8}$$

where Γ_e (mmol/g) is the equilibrium adsorption amount, C_i (mM) and C_e (mM) are the initial and remaining (equilibrium) concentrations, respectively, and C_s (g/L) is the adsorbent dosage.

For pH effect tests, the pH values of the adsorption systems were adjusted using NaOH and HCl solutions during the adsorption procedures. Other tests were performed at free pH.

Each test run was performed in triplicate, and the final values were presented as an average of the three measurements. The relative error was less than 5%.

Results and discussion

Characterization of silica samples

The S-SiO_2 and L-SiO_2 samples show spherical particles, as observed using TEM and SEM (Fig. 1). Their mean diameters (D_m), measured from the TEM and SEM images, are ~ 12 and 31 nm, respectively. The A_s values of the S-SiO_2 and L-SiO_2 were determined using the BET method to be 235 and 164 m^2/g (Fig. S2, ESM), respectively. The Si/O molar ratios of the two SiO_2 samples were determined by EDS all to be 0.49 ± 0.01, and no metallic elements are detectable, suggesting that the two samples have an extremely high purity and their surface hydroxyl groups exist in the neutral state (Sur-OH).

The acid-base titration was performed at 298 K for the silica samples, and the data were analyzed using the Gran function method (Fig. S3, ESM). The so-obtained N_s values of the S-SiO_2 and L-SiO_2 are 0.72 and 0.48 mmol/g (or 3.06 and 2.93 μmol/m^2, or 1.83 and 1.82 sites/nm^2), respectively, which are consistent with the literature values (2.3–10 μmol/m^2) [38, 59–61]. The two silica samples have the same surface hydroxyl density (~ 1.8 sites/nm^2). In addition, the N_s values suggest that the maximum surface charge densities (σ_m, those at $\alpha_{SH} = 1$) of the S-SiO_2 and L-SiO_2 are about − 0.29 and − 0.28 C/m^2, respectively.

The change in α_{SH} with pH for the S-SiO_2 and L-SiO_2 was estimated (Fig. S4, ESM). The results show that the dissociation of surface hydroxyl groups for the silica samples obviously occurs at pH higher than ~ 6, similar to the literature reports [3, 38, 60]. It is worth to note that the pH at which the α_{SH} begins to increase for the S-SiO_2 (pH ~ 6.0) is slightly lower than that for the L-SiO_2 (pH ~ 6.5), suggesting that the dissociation tendency of surface hydroxyl groups for the S-SiO_2 is stronger than that for the L-SiO_2. Based on the α_{SH} data, the pK_a values of the S-SiO_2 and L-SiO_2 are obtained at $\alpha_{SH} = 0.5$ to be 9.43 and 9.57, respectively, which are similar to the literature values (~ 7–10) [60]. The pK_a value of the S-SiO_2 is slightly lower than that of the L-SiO_2. A low pK_a value represents a strong dissociation tendency of the surface hydroxyl groups. Therefore, the pK_a data, along with the α_{SH} data, suggest that the surface hydroxyl groups of the S-SiO_2 exhibit a higher dissociation tendency than those of the L-SiO_2. Furthermore, these results also suggest that the affinity of the S-SiO_2 for cationic species may be weaker than that of the L-SiO_2, which is confirmed by the results of BDDABr adsorption tests. For clarity, the characterization results of the two silica samples are summarized in Table 1.

Micellization behavior of BDDABr in water

To understand the difference between the micellization of surfactant at solid–liquid interfaces and that in bulk solutions, the micellization behavior of BDDABr in bulk water was examined through conductivity (κ) measurements at three T (298, 303, and 308 K). Each plot of κ versus BDDABr concentration (C_0) at a given T exhibits two straight lines with different slopes (Fig. S5, ESM). The slope change arises from the formation of micelles, thereby the concentration corresponding to the intersection point between the two straight lines is assigned to the critical micelle concentration (*cmc*) [53]. In addition, the degree of micellar counterion dissociation (α_m) can be estimated from the ratio between the slopes of the κ–C_0 lines above and below *cmc* [53]. The *cmc* and α_m values of BDDABr in water are listed in Table 2 (and Fig. S6, ESM),

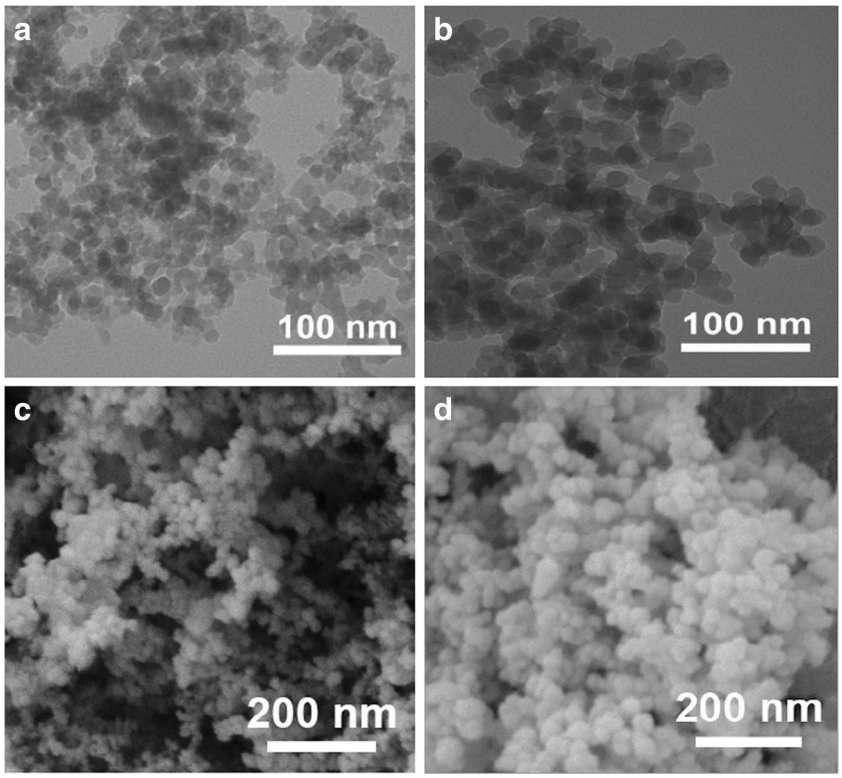

Fig. 1 **a**,**b** TEM and **c**,**d** SEM images of **a**,**c** S-SiO_2 and **b**,**d** L-SiO_2

which are close to the literature values [37, 53]. An increase in T leads to a rise of both *cmc* and α_m values, which is consistent with the previous report [53].

The thermodynamic parameters, including the standard Gibbs free energy ($\Delta\tilde{G}_m^\circ$), enthalpy ($\Delta\tilde{H}_m^\circ$), and entropy ($\Delta\tilde{S}_m^\circ$), for the micelle formation per mole of BDDABr can be calculated from the *cmc* and α_m values using the following equations:

$$\Delta\tilde{G}_m^\circ = (2-\alpha_m)RT\ln X_{cmc} \quad (9)$$

$$\Delta\tilde{H}_m^\circ = -(2-\alpha_m)RT^2\frac{d\ln X_{cmc}}{dT} \quad (10)$$

$$\Delta\tilde{S}_m^\circ = \frac{\Delta\tilde{H}_m^\circ - \Delta\tilde{G}_m^\circ}{T} \quad (11)$$

where X_{cmc} is the *cmc* in terms of mole fraction, R is the gas constant (8.314 J/(mol K)), and T (K) is the absolute temperature. The values of the micellization thermodynamic parameters are also listed in Table 2. The negative $\Delta\tilde{G}_m^\circ$ values indicate the thermodynamically spontaneous nature of the micellization, and the slight decrease in the absolute values of $\Delta\tilde{G}_m^\circ$ with increasing T indicates that a high T is unfavorable for the micellization. The negative $\Delta\tilde{H}_m^\circ$ value indicates that the micellization process is exothermic in nature. The positive $\Delta\tilde{S}_m^\circ$ value arises from the release of solvated water molecules during the micellization process. The negative $\Delta\tilde{H}_m^\circ$ and positive $\Delta\tilde{S}_m^\circ$ values together reveal that the micellization is driven by both enthalpy and entropy. Owing to the absolute value of $\Delta\tilde{H}_m^\circ$ being lower than that of $-T\Delta\tilde{S}_m^\circ$, the micellization can be considered to be mainly entropy-driven. These results are similar to the previous report [53].

Table 1 Basic properties of the silica samples

Sample	S-SiO_2	L-SiO_2
D_m (nm)	12	31
A_s (m^2/g)	235	164
N_s (mmol/g)	0.72	0.48
(μmol/m^2)	3.06	2.93
pK_a	9.43	9.57
σ_m (C/m^2)	− 0.29	− 0.28

Adsorption isotherms

Effect of adsorbent dosage and particle size The effect of silica dosages (C_s) on the BDDABr adsorption was examined at free pH and 298 K, as shown in Fig. 2. Obviously, the adsorption isotherms for the two silica samples are all independent of C_s, demonstrating that no C_s-effect exists in the adsorption under the studied conditions. Actually, previous reports on the C_s-effect are all associated with the adsorption of heavy metal ions or non-active organic substances at solid–liquid interfaces [55, 56], and there have been no reports about the C_s-effect existing in surfactant adsorption. Whether this is a feature of surfactant adsorption remains to be examined.

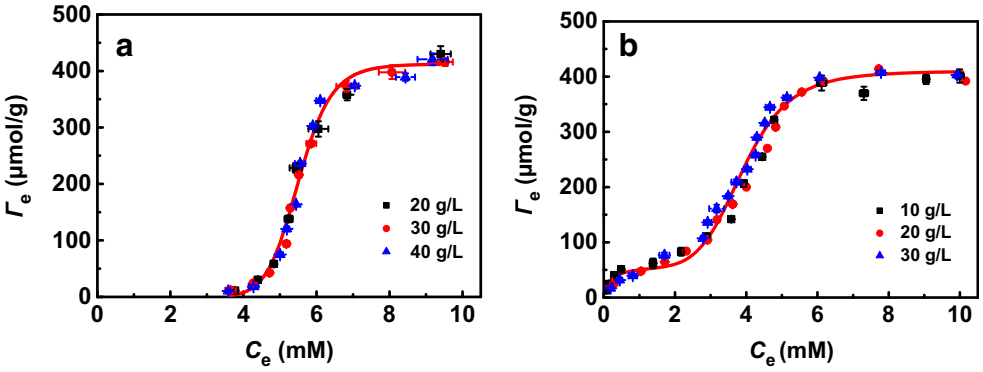

Fig. 2 Adsorption isotherms of BDDABr onto **a** S-SiO_2 and **b** L-SiO_2 at different C_s ($T = 298$ K, free pH)

Interestingly, it can be seen from Fig. 2 that the S-SiO_2 and L-SiO_2 exhibit different types of isotherms, namely, S-type and LS-type, respectively. An obvious double-plateau adsorption is observed for the L-SiO_2, while for the S-SiO_2, only at C_i higher than a given value (~3.5 mM), the adsorption obviously occurs. This suggests that the affinity of the S-SiO_2 toward BDDABr is lower than that of the L-SiO_2, which is consistent with the affinity of the two solids toward H^+ ions, as suggested by their pK_a values. In addition, the particle size-dependence of adsorption affinity observed here seems to be similar to those reported in the literature [47, 48] for adsorption of chicken egg lysozyme on silica nanoparticles [47] and HSA on NIPAM/BAM copolymer nanoparticles [48].

Notably, the above results are obtained at free pH. We noted that the free pH values of the S-SiO_2 and L-SiO_2 dispersions in equilibrium are different, being ~4.7 and 7.2, respectively, at a C_s of 20 g/L, which can be mainly attributed to the difference in the dissociation tendency of their surface hydroxyl groups. In addition, we also noted that, with the BDDABr adsorption, the free pH values of the S-SiO_2 and L-SiO_2 dispersions decrease to ~3.8 and 5.4 (Fig. S7, ESM), respectively, showing the adsorption is accompanied by the dissociation (or H^+ release) of solid surface hydroxyl groups. Similar results were reported in the literature for the adsorption of cationic surfactants on silica in water [37, 39, 41, 42]. Therefore, the effect of particle size on the adsorption observed at free pH includes the effect of pH changes caused by the change in particle sizes. To further understand the difference in adsorption for the two silica samples, the adsorption was determined under controlled pH conditions.

Effect of pH The change in the Γ_e with pH was first determined for the two silica samples at $C_i = 30$ mM, $C_s = 20$ mg/L, and $T = 298$ K, as shown in Fig. 3. The C_i of 30 mM corresponds to the maximum adsorption for the adsorption systems at various pH. It can be seen from Fig. 3 that, with increasing pH from ~3 to 10, the Γ_e values gradually increase, but which shows three successive stages. Initially, at pH < 4, the change of Γ_e with pH is very small (or the Γ_e keeps almost constant). Subsequently, at pH higher than ~4, the Γ_e shows a sharp increase. Finally, at pH higher than ~7, the Γ_e reaches a plateau. Notably, at pH higher than ~9.5, the Γ_e shows a slight increase, probably arising from the screening effect of electrolyte (NaOH) for the adsorption force [20] and the competitive adsorption of Na^+ with $BDDA^+$. The adsorption force of BDDABr on silica arises mainly from the electrostatic interaction between the cationic species $BDDA^+$ and the negatively charged surface sites (Sur-O^-). A high pH results in a high α_{SH} value, thereby in a high Γ_e value. Actually, the change in the Γ_e with pH is similar to that in the α_{SH} (Fig. S4, ESM), but the BDDABr adsorption facilitates the dissociation of surface hydroxyl groups. The plateau adsorption appearing at pH > 7 corresponds most likely to the complete dissociation of surface hydroxyl groups (i.e., $\alpha_{SH} = 1$).

The Γ_e values of the S-SiO_2 and L-SiO_2 at low pH (< 4) are ~494 and 425 μmol/g (or ~2.13 and 2.44 μmol/m^2), respectively, and those at high pH (> 7) are ~959 and 578 μmol/g (or ~4.08 and 3.52 μmol/m^2), respectively. Partyka et al. [37, 39] reported that, at pH ~4.1 and 6.7, the maximum Γ_e values of BDDABr on a silica with 130 nm in size were ~2.08 and 4.32 μmol/m^2, respectively. Our Γ_e values are close to the

Table 2 Micellization parameters of BDDABr in water at different T

T (K)	cmc (mM)	α_m	$\Delta\tilde{G}_m^\circ$ (kJ/mol)	$\Delta\tilde{H}_m^\circ$ (kJ/mol)	$\Delta\tilde{S}_m^\circ$ (kJ/(mol K))	$-T\Delta\tilde{S}_m^\circ$ (kJ/mol)
298	5.56	0.32	−38.32	−13.64	0.083	−24.73
303	5.86	0.35	−38.05	−13.85	0.080	−24.24
308	6.18	0.38	−37.75	−14.05	0.077	−23.72

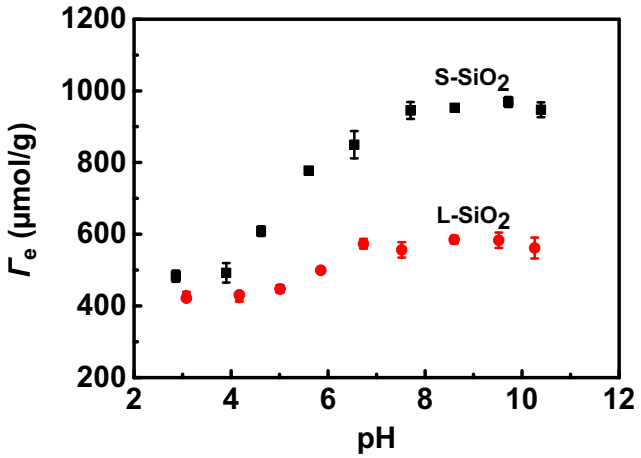

Fig. 3 Adsorption amounts of BDDABr onto S-SiO_2 and L-SiO_2 as a function of pH at $C_i = 30$ mM, $C_s = 20$ mg/L, and $T = 298$ K

literature values. In addition, for our two silica samples, the adsorption amounts per unit area (μmol/m^2) are close to each other, indicating that the higher adsorption amounts per unit mass (μmol/g) of the S-SiO_2 result mainly from its larger A_s. The area occupied per BDDABr molecule at water–gas interfaces ($a_{L\text{-}G}$) was reported to be ~0.71 nm^2 [37], where the BDDABr molecule can be regarded in a "fully" hydrated state. The intrinsic cross-sectional area of a BDDABr molecule (a_0, without hydration) is estimated using the molecular mechanic method to be ~0.54 nm^2. The $a_{L\text{-}G}$ and a_0 values suggest that the maximum adsorption capacity of a saturated adsorption monolayer should be in the range of ~2.34–3.08 μmol/m^2. Therefore, our Γ_e data suggest that the adsorption of BDDABr on the two adsorbents form a monolayer (or small, isolated surface micelle) structure at low pH (< 4) and a bilayer structure at high pH (> 7). If this is true, the areas occupied per BDDABr molecule ($a_{S\text{-}L}$) in the monolayers at low pH and in the bilayers at high pH are estimated all to be ~0.77 nm^2, which is close to its $a_{L\text{-}G}$ value (~0.71 nm^2). A similar $a_{S\text{-}L}$ value (~0.8 nm^2) was reported by Partyka et al. [39] for BDDABr adsorption on 130 nm silica particles at free pH. Such high $a_{S\text{-}L}$ value (close to the $a_{L\text{-}G}$ value) suggests that the adsorbed layers are less compact. It has been revealed that, at $C_e > cmc$, the adsorption of surfactant molecules at solid–liquid interfaces commonly forms a bilayer structure [5, 62, 63] and that the adsorption generally leads to a strong dehydration of the surfactant molecules (or a low $a_{S\text{-}L}$ value) [62, 63]. Therefore, it might be more reasonable to consider that all the adsorption layers at both low and high pH consist of isolated surface micelles, namely, isolated admicelles (or noncomplete bilayers [39]).

To understand the effect of pH on the isotherm types, the adsorption of BDDABr on the S-SiO_2 and L-SiO_2 at controlled pH of 4.0, 5.4, and 9.0 was determined at C_s = 20 mg/L and $T = 298$ K, as shown in Fig. 4. The isotherms at pH 9.0 for both the two silica samples can be recognized as LS-type or as L-type owing to the fact that the first-step adsorption is not very apparent. Therefore, a changing trend in isotherm types, namely, from S-type through LS-type to L-type, is observed with increasing pH under the studied conditions. This indicates that the affinity of the adsorbents toward BDDABr increases with a raise of pH, which arises from the increase in the negative charges of solid surfaces. In addition, it can be seen from Fig. 4 that the difference of isotherm types between the S-SiO_2 and L-SiO_2 appears only at low pH (especially at pH = 4.0). A possible reason for this result is that, at high pH, the large surface density of ionized surface hydroxyl groups (Sur-O^-) masks the effect of particle sizes on the adsorption.

Effect of temperature The effect of temperature on the adsorption of BDDABr onto the S-SiO_2 (pH 4.0) and L-SiO_2 (pH 5.4) was determined, as shown in Fig. 5. At the three T (298, 303, and 308 K) studied, the isotherms of the S-SiO_2 all are S-type, while those of the L-SiO_2 all are LS-type. That is, the change in T in the studied range has no influence on the isotherm type for each adsorbent. Interestingly, with increasing T from 298 to 308 K, the maximum Γ_e value of the S-SiO_2 exhibits an obvious decrease from ~361 to 231 μmol/g, while that of the L-SiO_2 exhibits a very slight decrease from ~410 to 375 μmol/g. Partyka et al. [37] reported that the maximum Γ_e values of BDDABr on large silica particles (130 nm in size) at free pH (~6.7) decreased

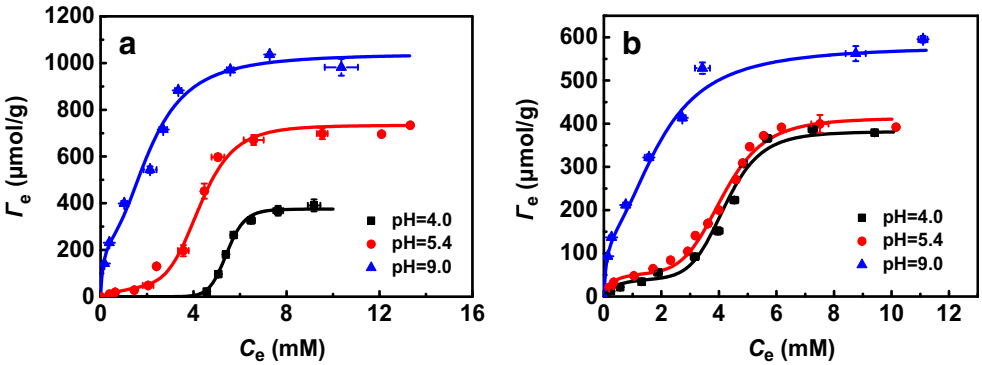

Fig. 4 Adsorption isotherms of BDDABr onto **a** S-SiO_2 and **b** L-SiO_2 at various controlled pH. $T = 298$ K, $C_s = 20$ g/L. The dots represent the experimental data, and the solid lines represent model fitting

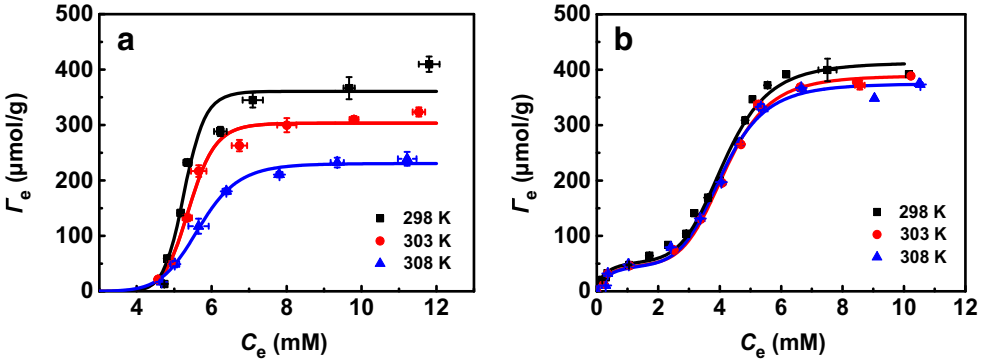

Fig. 5 Adsorption isotherms of BDDABr onto **a** S-SiO_2 (pH 4.0) and **b** L-SiO_2 (pH 5.4) at various T and C_s = 20 g/L. The dots represent the experimental data, and the solid lines represent model fitting

slightly from ~173 to 160 μmol/g with an increase in T from 298 to 308 K. Our results are similar to the previous report [37]. The reason for the difference in the T-dependence of adsorption amounts for the S-SiO_2 and L-SiO_2 is not clear. A possible explanation is that the stronger affinity of the L-SiO_2 for BDDABr results in the weaker effect of T on the adsorption.

Surface micellization model analysis

Theoretical basis

To understand the surface micellization behavior, the obtained S-type and LS-type isotherms were analyzed using the one-step and two-step models, respectively. For clarity, the theoretical bases of the two models are summarized as follows:

One-step model The one-step model [1, 11] supposes that the adsorption of surfactants at solid–liquid interfaces occurs in one step. That is, surfactant monomers adsorb on a surface site to directly form a surface micelle. The adsorption equilibrium can be represented as:

$$Site + n\,Monomer \rightleftharpoons Surface\ micelle \tag{12}$$

and its equilibrium constant, K_{os}, is:

$$K_{os} = \frac{a_{sm}}{a_s a_m^n} \tag{13}$$

where n is the average aggregation number of surface micelles, and a_s, a_m, and a_{sm} are the activities of unoccupied surface sites, free monomers, and surface micelles, respectively. For dilute adsorption systems, $a = C$. An isotherm equation of the one-step model can be derived as:

$$\Gamma_e = \frac{\Gamma_\infty K_{os} C_e^n}{1 + K_{os} C_e^n} \tag{14}$$

where Γ_∞ is the limiting adsorption amount.

Two-step model The two-step model [1, 12–14] supposes that the adsorption of surfactants at solid–liquid interfaces occurs in two steps. In the first step, surfactant monomers adsorb on solid surface sites as individuals through electrostatic attraction and/or specific (i.e., van der Waals) attraction, and no aggregates form. The first-step adsorption equilibrium can be represented as:

$$Site + Monomer \rightleftharpoons Adsorbed\ monomer \tag{15}$$

and its equilibrium constant, k_1, is:

$$k_1 = \frac{a_{am}}{a_s a_m} \tag{16}$$

where a_{am} is the activity of adsorbed monomers.

In the second step, free surfactant monomers adsorb on the previously adsorbed monomers through hydrophobic interaction between tails of surfactants, to form surface micelles. The second-step adsorption equilibrium can be represented as:

$$(n\text{–}1)\ Monomers + Adsorbed\ monomer \rightleftharpoons Surface\ micelle \tag{17}$$

and its equilibrium constant, k_2, is:

$$k_2 = \frac{a_{sm}}{a_{am} a_m^{n-1}} \tag{18}$$

A general isotherm equation of the two-step model can be derived as:

$$\Gamma_e = \frac{\Gamma_\infty k_1 C_e \left(\frac{1}{n} + k_2 C_e^{n-1}\right)}{1 + k_1 C_e \left(1 + k_2 C_e^{n-1}\right)} \tag{19}$$

Notably, the two-step isotherm has two important limiting cases [1, 14]. If $k_2 \rightarrow 0$ and $n \rightarrow 1$, it reduces to the Langmuir

isotherm. If $n > 1$ and $k_1 C_e \ll 1$, it reduces to the one-step isotherm. Therefore, the Langmuir and one-step models can be regarded as two limiting cases of the more general two-step model.

Critical surface micelle concentration The critical surface micelle concentration (*csmc*) is defined as the concentration at which surface micelles begin to form on the solid surface and can be estimated from model parameter values using the following equations [1, 14]:

$$for\ \text{S-}type\ isotherm, csmc = \left(\frac{n-1}{n+1}\right)^{(n+1)/n} K_{os}^{-1/n} \quad (20)$$

$$for\ \text{LS-}type\ isotherm, csmc = \left(\frac{n-2}{n}\right)^{n/(n-1)} k_2^{1/(1-n)} \quad (21)$$

Thermodynamics of surface micellization From the equilibrium constants of adsorption, the standard Gibbs free energy of surface micellization per mole of surfactant ($\Delta\tilde{G}_{sm}^{\circ}$) can be calculated using the following equations [1, 14]:

for S-type isotherm,

$$\Delta\tilde{G}_{sm}^{\circ} = -\frac{1}{n} RT \ln K_{os} \quad (22)$$

for LS-type isotherm,

$$\Delta\tilde{G}_{sm}^{\circ} = -\frac{1}{n} RT \ln k_2 \quad (23)$$

The standard entropy ($\Delta\tilde{S}_{sm}^{\circ}$) and enthalpy ($\Delta\tilde{H}_{sm}^{\circ}$) of surface micellization per mole of surfactant can be calculated using the following equations [1, 14]:

$$\Delta\tilde{S}_{sm}^{\circ} = -\frac{d\Delta\tilde{G}_{sm}^{\circ}}{dT} \quad (24)$$

$$\Delta\tilde{H}_{sm}^{\circ} = \Delta\tilde{G}_{sm}^{\circ} + T\Delta\tilde{S}_{sm}^{\circ} \quad (25)$$

Modeling for adsorption data

The fitting procedure of surface micellization models for adsorption data was performed using the 1stOpt software with the Levenberg-Marquardt algorithm. The best-fit values of model parameters for a set of $\Gamma_e - C_e$ data (or an isotherm) were automatically obtained from the software, which correspond to the minimum sum of square of residuals, $SS_{residuals} = \Sigma(\Gamma_{cal} - \Gamma_{exp})^2$, where Γ_{cal} and Γ_{exp} are the calculated and experimental adsorption amounts, respectively.

The fitting plots of the one-step and two-step models for the adsorption data are shown in Figs. 2, 4, and 5. All of the model plots coincide well with the experimental data, demonstrating that the one-step and two-step models can adequately describe the S-type and LS-type isotherms, respectively, obtained for the adsorption systems. The best-fit values of the model parameters and the correlation coefficient (R^2) are listed in Tables 3 and 4 (and Tables S1 and S2, ESM). Notably, the expressed unit of concentration (mmol/L) in the K_{os} ((mmol/L)$^{-n}$), k_1 ((mmol/L)$^{-1}$), and k_2 ((mmol/L)$^{-(n-1)}$) is converted to mole fraction (mol/mol) for calculation of $\Delta\tilde{G}_{sm}^{\circ}$ using Eqs. (22) and (23). In addition, the isotherms at pH 9.0 for the S-SiO_2 and L-SiO_2 were also fitted using the Langmuir model (see Section S1, Fig. S8, and Table S3, ESM), showing that they can be described also using the Langmuir model, namely, can also be recognized as L-type. However, it is better to recognize the two isotherms as LS-type owing to the maximum adsorption amounts (Γ_m) obtained from the Langmuir model (1230 and 723 μmol/g) being obviously higher than the experimental (Γ_∞) values (~ 1040 and 580 μmol/g).

From Tables 3 and 4, it can be seen that the *n* values obtained at different conditions are in the range of 3.16–16.1, which is consistent with the reported *n* values (3–20) for surface micelles in the literature [1, 14, 21]. With increasing pH, the *n* values for the two silica samples all decrease obviously (Table 3). Similar results were reported in the literature [1]. It can be seen from Table 3 that, for the LS-type adsorption, an increase in pH results in a rise of the first-step adsorption (Γ_1, see Table S1, ESM). Enough high Γ_1 may result in one surface micelle developing around more than one anchor chain [1], thereby resulting in a decrease in *n*. With increasing *T*, the *n* values for the two silica samples also decrease (Table 4), which is consistent with the previous report on BDDABr adsorption on silica [37] but contrary to the previous report on adsorption of the nonionic surfactant decylmethylsulphoxide (DEMS) on carbon black [13]. We noted that the Γ_∞ values of DEMS on carbon black increase with increasing *T* [13]. However, for the adsorption of BDDABr on silica, an opposite change in Γ_∞ with *T* occurs. Therefore, our result is reasonable. In addition, the *T*-dependence of *n* values for BDDABr observed here is similar to the reports for ionic surfactants in bulk solutions [64, 65]. Notably, the change of the *n* value for the L-SiO_2 with *T* is very small, which is probably related to the small change in its Γ_1 and Γ_∞ values.

The *csmc* values obtained at different conditions are in the range of 0.47–4.69 mM (Tables 3 and 4), which is obviously lower than the *cmc* of BDDABr in bulk water (5.56–6.18 mM). This is a feature of surface micellization of surfactants [1, 14, 21, 28]. With increasing pH, the *csmc* values on the two silica samples obviously decrease (Table 3). Pham et al. [21] reported that the *csmc* values for adsorption of the

Table 3 Best-fit values of model parameters for BDDABr adsorption on S-SiO_2 and L-SiO_2 at different pH (T = 298 K)

Adsorbent	S-SiO_2			L-SiO_2		
pH (± 0.2)	4.0	5.4	9.0	4.0	5.4	9.0
Isotherm type	S	LS	LS	LS	LS	LS
Γ_∞ (μmol/g)	360.7	733.7	1040	381.8	410.0	580.0
n	16.1	8.07	3.47	7.71	6.93	3.16
k_1	/	4.35×10^4	3.85×10^5	1.34×10^5	3.07×10^5	4.19×10^5
k_2	/	1.50×10^{29}	7.34×10^{10}	4.69×10^{27}	4.21×10^{24}	3.72×10^9
K_{os} or K_{ts}	5.93×10^{64}	6.53×10^{33}	2.80×10^{16}	6.28×10^{32}	1.29×10^{30}	1.32×10^{15}
csmc (mM)	4.62	2.99	0.66	3.05	2.66	0.47
R^2	0.9171	0.9880	0.9928	0.9954	0.9868	0.9932
$\Delta\tilde{G}^\circ_{sm}$ (kJ/mol)	− 22.95	− 20.63	− 17.86	− 20.47	− 20.12	− 17.28

anionic surfactant sodium dodecyl sulfate (SDS) on α-Al_2O_3 increase with increasing pH. It should be noted that, with increasing pH, the affinity of SDS toward α-Al_2O_3 decreases while that of BDDABr toward silica increases. Therefore, the result of the *csmc* values decreasing with pH obtained here can be attributed to the enhancement of the affinity between BDDABr and silica. With increasing T, the *csmc* values on the two silica samples slightly increase (Table 4), which is similar to the change of *cmc* of BDDABr in bulk water.

The $\Delta\tilde{G}^\circ_{sm}$ and $\Delta\tilde{H}^\circ_{sm}$ values obtained at different conditions are negative and the obtained $\Delta\tilde{S}^\circ_{sm}$ values are positive (Tables 3 and 4), which are the same as the case of micellization of BDDABr in bulk water. Notably, the absolute values of $\Delta\tilde{G}^\circ_{sm}$ (17.28–23.49 kJ/mol) are lower than those of $\Delta\tilde{G}^\circ_{m}$ of BDDABr in bulk water (37.75–38.32 kJ/mol). One possible reason is that the degree of counterion dissociation of surface micelles is not taken into account in the one-step and two-step models. In addition, the absolute values of $\Delta\tilde{H}^\circ_{sm}$ are obviously lower than that of $-T\Delta\tilde{S}^\circ_{sm}$, demonstrating that the surface micellization is mainly entropy-driven, which is similar to the bulk micellization. With increasing pH, the absolute values of $\Delta\tilde{G}^\circ_{sm}$ for the two silica samples all decrease (Table 3), suggesting the surface micellization tendency becomes weaker. With increasing T, the absolute values of $\Delta\tilde{G}^\circ_{sm}$ for the two silica samples all slightly increase (Table 4), suggesting the surface micellization tendency becomes stronger, which is contrary to the bulk micellization. Furthermore, we can see from Table 3 that, at given pH and T, the n and *csmc* values of the S-SiO_2 are higher than those of the L-SiO_2, demonstrating that the affinity of the S-SiO_2 toward BDDABr is lower than that of the L-SiO_2. The model fitting result is consistent with the results of isotherm type observations and pK_a determinations.

Conclusions

The adsorption of BDDABr on two silica samples, S-SiO_2 and L-SiO_2, in water was investigated. No C_s-effect is observed

Table 4 Best-fit values of model parameters for BDDABr adsorption on S-SiO_2 (pH 4.0) and L-SiO_2 (pH 5.4) at different T

Adsorbent	S-SiO_2			L-SiO_2		
T (K)	298	303	308	298	303	308
Isotherm type	S	S	S	LS	LS	LS
Γ_∞ (μmol/g)	360.7	303.3	230.6	410.0	388.8	375.3
n	16.1	13.1	10.8	6.93	6.81	6.80
k_1	/	/	/	3.07×10^5	1.63×10^5	1.58×10^5
k_2	/	/	/	4.21×10^{24}	9.48×10^{23}	8.12×10^{23}
K_{os} or K_{ts}	5.93×10^{64}	2.82×10^{52}	1.09×10^{43}	1.29×10^{30}	1.55×10^{29}	6.84×10^{28}
csmc (mM)	4.62	4.67	4.69	2.66	2.76	2.78
R^2	0.9171	0.9763	0.9899	0.9868	0.9943	0.9922
$\Delta\tilde{G}^\circ_{sm}$ (kJ/mol)	− 22.95	− 23.22	− 23.49	− 20.27	− 20.42	− 20.77
$-T\Delta\tilde{S}^\circ_{sm}$ (kJ/mol)	− 16.09	− 16.36	− 16.63	− 14.90	− 15.15	− 15.40
$\Delta\tilde{H}^\circ_{sm}$ (kJ/mol)	− 6.86	− 6.86	− 6.86	− 5.37	− 5.27	− 5.37

for the adsorption, while the size of silica particles, besides pH and *T*, has an obvious impact on the adsorption. The S-SiO_2 shows a S-type isotherm while the L-SiO_2 shows a LS-type isotherm at low pH (~4.0). An increase in pH may lead to a change in the isotherm types from S-type through LS-type to L-type. The S-type and LS-type isotherms can be adequately described using the one-step and two-step models, respectively. With increasing pH, the *n* and *csmc* values all decrease. With increasing *T*, the *n* values decrease while the *csmc* values slightly increase. At given pH and *T*, the *n* and *csmc* values for the S-SiO_2 are obviously higher than those for the L-SiO_2. These results suggest that the affinity of the S-SiO_2 toward BDDABr is lower than that of the L-SiO_2, which is consistent with the dissociation tendency of their surface hydroxyl groups. This work provides a well understanding of the particle size-dependence of cationic surfactant adsorption at silica–liquid interfaces.

Acknowledgements This work was financially supported by the National Natural Science Foundation of China (No. 21573133).

Compliance with ethical standards

Conflict of interest The authors declare that they have no conflict of interest.

References

1. Gu T, Zhu BY, Rupprecht H (1992) Surfactant adsorption and surface micellization. Colloid Polym Sci 88:74–85. https://doi.org/10.1007/BFb0114420
2. Atkin R, Craig VSJ, Wanless EJ, Biggs S (2003) Mechanism of cationic surfactant adsorption at the solid–aqueous interface. Adv Colloid Interf Sci 103(3):219–304. https://doi.org/10.1016/S0001-8686(03)00002-2
3. Paria S, Khilar KC (2004) A review on experimental studies of surfactant adsorption at the hydrophilic solid–water interface. Adv Colloid Interf Sci 110(3):75–95. https://doi.org/10.1016/j.cis.2004.03.001
4. Parida SK, Dash S, Patel S, Mishra BK (2006) Adsorption of organic molecules on silica surface. Adv Colloid Interf Sci 121(1-3):77–110. https://doi.org/10.1016/j.cis.2006.05.028
5. Zhang R, Somasundaran P (2006) Advances in adsorption of surfactants and their mixtures at solid/solution interfaces. Adv Colloid Interf Sci 123–126:213–229
6. Mu Q, Jiang G, Chen L, Zhou H, Fourches D, Tropsha A, Yan B (2014) Chemical basis of interactions between engineered nanoparticles and biological systems. Chem Rev 114(15):7740–7781. https://doi.org/10.1021/cr400295a
7. Tardy BL, Yokota S, Ago M, Xiang W, Kondo T, Bordes R, Rojas OJ (2017) Nanocellulose–surfactant interactions. Cur Opin Colloid Interface Sci 29:57–67
8. Khobragade MU, Pal A (2016) Adsorptive removal of Mn(II) from water and wastewater by surfactant-modified alumina. Desalination Water Treat 57(6):2775–2786. https://doi.org/10.1080/19443994.2014.982195
9. Pham TD, Do TT, Ha VL, Doan THY, Nguyen TAH, Mai TD, Kobayashi M, Adachi Y (2017) Adsorptive removal of ammonium ion from aqueous solution using surfactant-modified alumina. Environ Chem 14(5):327–337. https://doi.org/10.1071/EN17102
10. Pham TD, Nguyen HH, Nguyen NV, Vu TT, Pham TNM, Doan THY, Nguyen MH, Ngo, TMV (2017) Adsorptive removal of copper by using surfactant modified laterite soil. J Chem 2017: ID 1986071, https://doi.org/10.1155/2017/1986071
11. Gu T, Zhu BY (1990) The S-type isotherm equation for adsorption of nonionic surfactants at the silica gel–water interface. Colloids Surf 44:81–87. https://doi.org/10.1016/0166-6622(90)80189-B
12. Zhu BY, Gu T (1989) General isotherm equation for adsorption of surfactants at solid/liquid interfaces. Part 1. Theoretical. J Chem Soc Faraday Trans I 85(11):3813–3817. https://doi.org/10.1039/f19898503813
13. Zhu BY, Gu T, Zhao X (1989) General isotherm equation for adsorption of surfactants at solid/liquid interfaces. Part 2. Applications. J Chem Soc Faraday Trans I 85(11):3819–3824. https://doi.org/10.1039/f19898503819
14. Zhu BY, Gu T (1991) Surfactant adsorption at solid–liquid interfaces. Adv Colloid Interf Sci 37(1-2):1–32. https://doi.org/10.1016/0001-8686(91)80037-K
15. Scamehorn JF, Schechter RS, Wade WH (1982) Adsorption of surfactants on mineral oxide surfaces from aqueous solutions: I: Isomerically pure anionic surfactants. J Colloid Interface Sci 85(2):463–478. https://doi.org/10.1016/0021-9797(82)90013-3
16. Böhmer MR, Koopal LK (1992) Adsorption of ionic surfactants on variable-charge surfaces. 1. Charge effects and structure of the adsorbed layer. Langmuir 8(11):2649–2659. https://doi.org/10.1021/la00047a014
17. Koopal LK, Lee EM, Böhmer MR (1995) Adsorption of cationic and anionic surfactants on charged metal oxide surfaces. J Colloid Interface Sci 170(1):85–97. https://doi.org/10.1006/jcis.1995.1075
18. Pham TD, Kobayashi M, Adachi Y (2013) Interfacial characterization of α-alumina with small surface area by streaming potential and chromatography. Colloids Surf A Physicochem Eng Asp 436:148–157. https://doi.org/10.1016/j.colsurfa.2013.06.026
19. Pham TD, Kobayashi M, Adachi Y (2014) Adsorption of polyanion onto large alpha alumina beads with variably charged surface. Adv Phys Chem 2014: ID 460942, doi: https://doi.org/10.1155/2014/460942
20. Pham TD, Kobayashi M, Adachi Y (2015) Adsorption characteristics of anionic azo dye onto large α-alumina beads. Colloid Polym Sci 293(7):1877–1886. https://doi.org/10.1007/s00396-015-3576-x
21. Pham TD, Kobayashi M, Adachi Y (2015) Adsorption of anionic surfactant sodium dodecyl sulfate onto alpha alumina with small surface area. Colloid Polym Sci 293(1):217–227. https://doi.org/10.1007/s00396-014-3409-3
22. Yang YJ, Corti DS, Franses EI (2017) Effect of Triton X-100 on the stability of titania nanoparticles against agglomeration and sedimentation: a masked depletion interaction. Colloids Surf A Physicochem Eng Asp 516:l296–l304
23. Roth HC, Schwaminger S, García PF, Ritscher J, Berensmeier S (2016) Oleate coating of iron oxide nanoparticles in aqueous systems: the role of temperature and surfactant concentration. J Nanopart Res 18(4):99–110. https://doi.org/10.1007/s11051-016-3405-2
24. Wood MH, Casford MT, Steitz R, Zarbakhsh A, Welbourn RJL, Clarke SM (2016) Comparative adsorption of saturated and unsaturated fatty acids at the iron oxide/oil interface. Langmuir 32(2):534–540. https://doi.org/10.1021/acs.langmuir.5b04435
25. Reid MS, Villalobos M, Cranston ED (2017) The role of hydrogen bonding in non-ionic polymer adsorption to cellulose nanocrystals and silica colloids. Cur Opin Colloid Interface Sci 29:76–82
26. Meissner J, Prause A, Bharti B, Findenegg GH (2015) Characterization of protein adsorption onto silica nanoparticles: influence of pH and ionic strength. Colloid Polym Sci 293(11):3381–3391. https://doi.org/10.1007/s00396-015-3754-x

27. Jayawardane D, Pan F, JR L, Zhao X (2015) Co-adsorption of peptide amphiphile V_6K and conventional surfactants SDS and C_{12}TAB at the solid-water interface. Soft Matter 11(40):7986–7994. https://doi.org/10.1039/C5SM01670C
28. Liu Y, Qiao L, Xiang Y, Guo R (2016) Adsorption behavior of low-concentration imidazolium-based ionic liquid surfactant on silica nanoparticles. Langmuir 32(11):2582–2590. https://doi.org/10.1021/acs.langmuir.6b00302
29. Saha R, Uppaluri RVS, Tiwari P (2017) Effect of mineralogy on the adsorption characteristics of surfactant–reservoir rock system. Colloids Surf A Physicochem Eng Asp 531:121–132. https://doi.org/10.1016/j.colsurfa.2017.07.039
30. Guégan R, Veron E, Forestier LL, Ogawa M, Cadars S (2017) Structure and dynamics of nonionic surfactant aggregates in layered materials. Langmuir 33(38):9759–9771. https://doi.org/10.1021/acs.langmuir.7b01831
31. Harkot J, Jańczuk B (2009) He role of adsorption of dodecylethyldimethylammonium bromide and benzyldimethyldodecylammonium bromide surfactants in wetting of polytetrafluoroethylene and poly(methyl methacrylate) surfaces. Appl Surf Sci 255(6):3623–3628. https://doi.org/10.1016/j.apsusc.2008.10.007
32. Yang Z, Tarabara VV, Bruening ML (2015) Adsorption of anionic or cationic surfactants in polyanionic brushes and its effect on brush swelling and fouling resistance during emulsion filtration. Langmuir 31(43):11790–11799. https://doi.org/10.1021/acs.langmuir.5b01938
33. Meconi GM, Ballard N, Asua JM, Zangi R (2016) Adsorption and desorption behavior of ionic and nonionic surfactants on polymer surfaces. Soft Matter 12(48):9692–9704. https://doi.org/10.1039/C6SM01878E
34. Moussavi G, Shekoohiyan S, Mojab S (2016) Adsorption capacity of NH_4Cl-induced activated carbon for removing sodium dodecyl sulfate from water. Desalination Water Treat 57(24):11283–11290. https://doi.org/10.1080/19443994.2015.1043955
35. Vo MD, Papavassiliou DV (2017) Effects of temperature and shear on the adsorption of surfactants on carbon nanotubes. J Phys Chem C 121(26):14339–14348. https://doi.org/10.1021/acs.jpcc.7b03904
36. Striolo A (2017) Surfactant assemblies on selected nanostructured surfaces: evidence, driving forces, and applications. Langmuir 33(33):8099–8113. https://doi.org/10.1021/acs.langmuir.7b00756
37. Trompette JL, Zajac J, Keh E, Partyka S (1994) Scanning of the cationic surfactant adsorption on a hydrophilic silica surface at low surface coverages. Langmuir 10(3):812–818. https://doi.org/10.1021/la00015a036
38. Goloub TP, Koopal LK, Bijsterbosch BH (1996) Adsorption of cationic surfactants on silica. Surface charge effects. Langmuir 12(13):3188–3194. https://doi.org/10.1021/la9505475
39. Zajac J, Trompette JL, Partyka S (1996) Adsorption of cationic surfactants on a hydrophilic silica surface at low surface coverages: effects of the surfactant alkyl chain and exchangeable sodium cations. Langmuir 12(5):1357–1367. https://doi.org/10.1021/la950645q
40. Goloub TP, Koopal LK (1997) Adsorption of cationic surfactants on silica. Comparison of experiment and theory. Langmuir 13(4):673–681. https://doi.org/10.1021/la960690d
41. Chorro M, Chorro C, Dolladille O, Partyka S, Zana R (1999) Adsorption mechanism of conventional and dimeric cationic surfactants on silica surface: effect of the state of the surface. J Colloid Interface Sci 210(1):134–143. https://doi.org/10.1006/jcis.1998.5936
42. Grosmaire L, Chorro M, Chorro C, Partyka S (2001) Influence of the chemical surface state of silica on adsorption process of conventional cationic and Gemini surfactants: thermodynamic investigations. J Colloid Interface Sci 242(2):395–403. https://doi.org/10.1006/jcis.2001.7795
43. Ahualli S, Iglesias GR, Wachter W, Dulle M, Minami D, Glatter O (2001) Adsorption of anionic and cationic surfactants on anionic colloids: supercharging and destabilization. Langmuir 27:9182–9192
44. Cummins PG, Staples E, Penfold J (1991) Temperature dependence of the adsorption of hexaethylene glycol monododecyl ether (C12E6) on silica sols. J Phys Chem 95(15):5902–5905. https://doi.org/10.1021/j100168a035
45. Penfold J, Staples E, Tucker I, Cummins P (1996) Adsorption of nonionic surfactants on silica sol particles: the effects of sol type and concentration, surfactant type, concentration, and temperature. J Phys Chem 100(46):18133–18137. https://doi.org/10.1021/jp9611838
46. Greenwood R, Luckham PF, Gregory T (1995) The effect of particle size on the layer thickness of a stabilizing polymer adsorbed onto two different classes of polymer latex, as determined from rheological experiments. Colloids Surf A Physicochem Eng Asp 98(1-2):117–125. https://doi.org/10.1016/0927-7757(95)03114-S
47. Vertegel AA, Siegel RW, Dordick JS (2004) Silica nanoparticle size influences the structure and enzymatic activity of adsorbed lysozyme. Langmuir 20(16):6800–6807. https://doi.org/10.1021/la0497200
48. Lindman S, Lynch I, Thulin E, Nilsson H, Dawson KA, Linse S (2007) Systematic investigation of the thermodynamics of HSA adsorption to *N*-iso-propylacrylamide/*N*-tert-butylacrylamide copolymer nanoparticles. Effects of particle size and hydrophobicity. Nano Lett 7(4):914–920. https://doi.org/10.1021/nl062743+
49. Walkey CD, Olsen JB, Guo H, Emili A, Chan WCW (2012) Nanoparticle size and surface chemistry determine serum protein adsorption and macrophage uptake. J Am Chem Soc 134(4):2139–2147. https://doi.org/10.1021/ja2084338
50. Bull JP, Serreqi AN, Chen T, Breuil C (1998) Development of an immunoassay for a quaternary ammonium compound, benzyldimethyldodecylammonium chloride. Wat Res 32(12):3621–3630. https://doi.org/10.1016/S0043-1354(98)00127-4
51. Harkot J, Jańczuk B (2009) Surface and volume properties of dodecylethyldimethylammonium bromide and benzyldimethyldodecylammonium bromide I. Surface properties of dodecylethyldimethylammonium bromide and benzyldimethyldodecylammonium bromide. J Colloid Interface Sci 331(2):494–499. https://doi.org/10.1016/j.jcis.2008.11.064
52. Ferreira C, Pereira AM, Pereira MC, Melo LF, Simões M (2011) Physiological changes induced by the quaternary ammonium compound benzyldimethyldodecylammonium chloride on pseudomonas fluorescens. J Antimicrob Chemother 66(5):1036–1043. https://doi.org/10.1093/jac/dkr028
53. Ghosh KK, Baghel V (2008) Micellar properties of benzyldimethyldodecylammonium bromide in aquo-organic solvent media. Indian J Chem 47A:1230–1233
54. Harkot J, Jańczuk B (2009) Surface and volume properties of dodecylethyldimethylammonium bromide and benzyldimethyldodecylammonium bromide II. Volumetric properties of dodecylethyldimethylammonium bromide and benzyldimethyldodecylammonium bromide. J Colloid Interface Sci 330(2):467–473. https://doi.org/10.1016/j.jcis.2008.10.078
55. Zhao LX, Song SE, Du N, Hou WG (2013) A sorbent concentration-dependent Freundlich isotherm. Colloid Polym Sci 291(3):541–550. https://doi.org/10.1007/s00396-012-2742-7
56. Zhang F, Song Y, Song S, Zhang R, Hou W (2015) Synthesis of magnetite–graphene oxide-layered double hydroxide composites and applications for the removal of Pb (II) and 2, 4-dichlorophenoxyacetic acid from aqueous solutions. ACS Appl Mater Interfaces 7(13):7251–7263. https://doi.org/10.1021/acsami.5b00433
57. Jolsterå R, Gunneriusson L, Forsling W (2010) Adsorption and surface complex modeling of silicates on maghemite in aqueous

suspensions. J Colloid Interface Sci 342(2):493–498. https://doi.org/10.1016/j.jcis.2009.10.080
58. Wang LL, Wang LF, Ren XM, Ye XD, Li WW, Yuan SJ, Sun M, Sheng GP, Yu HQ, Wang XK (2012) pH dependence of structure and surface properties of microbial EPS. Environ Sci Technol 46(2):737–744. https://doi.org/10.1021/es203540w
59. Li L, Du X, Lu Y, Yang Z (2007) Study on the first-step adsorption of dodecyltrimethylammonium bromide solutions on silica wafer surfaces by ultramicroelectrode voltammetry. Electrochem Commun 9(9):2308–2314. https://doi.org/10.1016/j.elecom.2007.06.039
60. Zhang WM, Yang ZD, Liu J, Sun ZX (2010) Determination of acid-base equilibrium constants on aqueous mesoporous silica surfaces. Acta Phys -Chim Sin 26:2109–2114
61. Liu J, Zhang WM, Huang PP, Fan JN, Sun RG, Sun ZX (2011) Surface complexation reactions in a mixed α-Fe_2O_3, γ-Al_2O_3 and SiO_2 suspension. Acta Phys-Chim Sin 27:186–192
62. Zhu X, Du N, Song R, Hou W, Song S, Zhang R (2014) Rough glass surface-mediated formation of vesicles from lauryl sulfobetaine micellar solutions. Langmuir 30(39):11543–11551. https://doi.org/10.1021/la502965q
63. Song R, Du N, Zhu X, Li H, Song S, Hou W (2015) Rough glass surface-mediated transition of micelle-to-vesicle in sodium dodecylbenzenesulfonate solutions. J Phys Chem B 119(9):3762–3767. https://doi.org/10.1021/jp509795v
64. Roelants E, Geladé E, Smid J, De Schryver FC (1985) A study of temperature dependence of the mean aggregation number and the kinetic parameters of quenching in CTAC and TTAC micelles. J Colloid Interface Sci 107(2):337–344. https://doi.org/10.1016/0021-9797(85)90186-9
65. Zana R, Benrraou M, Bales BL (2004) Effect of the nature of the counterion on the properties of anionic surfactants. 3. Self-association behavior of tetrabutylammonium dodecyl sulfate and tetradecyl sulfate: clouding and micellar growth. J Phys Chem B 108(47):18195–18203. https://doi.org/10.1021/jp040507m